Vol. 47, No. 4 (2025) 692-704, DOI: 10.24874/ti.2023.09.25.11

Tribology in Industry

www.tribology.rs

RESEARCH

Eco-Friendly Ni-P-TiO_2 Composite Coatings on AH36 Steel Using Plant-Extracted Nanoparticles for Marine Corrosion Resistance

Ganta Suresh[a], T. Vinod Kumar[a], R. Muraliraja[a,*], Arumugam Padmapriya[b]

[a]*Vels Institute of Science Technology and Advanced Studies, Chennai-600117, India,*
[b]*Vinayaka Mission's Research Foundation (DU), Chennai Campus, Paiyanoor-603104, India.*

Keywords:

Steel
Coatings
Marine environment
Corrosion
Strength

* Corresponding author:

R. Muraliraja
E-mail: muralimechraja@gmail.com

Received: 16 September 2025
Revised: 11 October 2025
Accepted: 10 November 2025

A B S T R A C T

Marine grade AH36 steel, widely used in offshore and shipbuilding industry, tends to suffer severe corrosion from aggressive marine condition. In order to improve its corrosion resistance and mechanical hardness this research deals with the development of electroless Ni-P composite coatings reinforced with TiO_2 nanoparticles in three structural states: anatase, rutile and amorphous derived from plant extraction. A fourth hybrid specimen having all the three TiO_2 phases was also examined. The coatings were deposited on AH36 steel and analyzed by Scanning Electron Microscopy (SEM), X-Ray Diffraction (XRD), Atomic Force Microscopy (AFM), microhardness measurement and electrochemical Tafel polarization measurement. The sample containing anatase coating had the best performance, showing up to 27 µm thickness. The results indicate a 13.5% increase in performance compared with the Ni–P sample, 67.4 nm surface roughness, and 200 HV (25% increase) microhardness. It also showed the highest corrosion resistance, with the maximum corrosion potential (–0.65 V) and lowest corrosion current density, which means the lowest corrosion in the sample. In comparison, the amorphous Titanium di oxide (TiO_2) coating had a large surface roughness of 170.1 nm and lower coating thickness of 20 µm, where the hybrid sample was marked with the smallest coating thickness of 16 µm along with in homogeneous morphology. The rutile-type coating showed a mediocre performance with coating thickness of 24 µm and surface roughness of 106.6 nm. These results clearly demonstrate that the anatase phase is beneficial for homogeneous dispersal, large surface coverage and electrochemical protection. This work emphasises that TiO_2 phase is crucial in developing efficient electroless composite coatings for marine steel.

1. INTRODUCTION

Steel stands as one of the most prevalent materials used in marine engineering because of its remarkable mechanical behaviours, including high strength, durability, & cost-effectiveness. It's widely employed in building ships, offshore structures, pipelines, and harbor infrastructure. However, steel is quite prone to corrosion when subjected to harsh marine environments with high salinity, moisture, and varying temperatures. This situation makes strategies for preventing and protecting against corrosion crucial for ensuring that steel structures remain reliable and last longer in marine condition. Applications of steel in maritime contexts can generally be divided into several categories as illustrated in Figure 1.

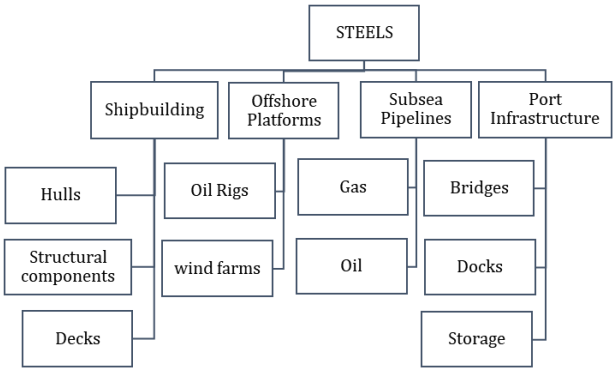

Fig. 1. Applications of AH36 steel in marine environment.

Steel is the most widely used material for marine engineering all over the world and has been employed for structural elements such as plates, profiles, and bars. AH36, a high-strength member steel used in the construction of shipbuilding and offshore platforms, has been commonly employed in shipbuilding and offshore structure due to the mechanical strength and resistance to the dynamic and static load in the marine environment. Nevertheless, one of the main disadvantages of steel used in marine environment is that it is prone to corrosion, particularly in the presence of salt which can act as an aggressive corrosion trigger [1,2]. Corrosion causes not only deterioration of materials themselves, but also the destruction of structures, increment of maintenance, and accident hazard. This problem assumes an added importance when considering marine applications, including ship hulls, offshore platforms, subsea pipelines and coastal infrastructure [3] where seawater, humidity and temperature changes are constant. Therefore, increasing the corrosion resistance of steel parts has become a major challenge for the maritime domain. Surface modification, especially protective coatings, has proven to be one of the potential methods to mitigate the problems related to corrosion in these harsh conditions [4]. Improving steel's ability to fend off rust has become a big deal for the maritime world. Surface engineering, with a focus on protective coatings, is now seen as a key way to tackle rust problems in tough environments. Electroless nickel-phosphorus (Ni-P) plating is superior in protecting the material from harsh environments because it forms reliable coatings on complex shapes and inner surface of the pipelines [5]. This process uses the autocatalytic reduction of nickel ions with a chemical called reducing agent, usually sodium hypophosphite, in a water-based solution. Compared to bare steel, the Ni-P layer gives a notable boost in wear resistance, hardness & rust protection [6]. Incorporation of hard ceramic particles like TiO_2 into the electroless Ni–P matrix results in the formation of a composite coating. This offers better mechanical and electrochemical perquisites [7]. TiO_2 is known all around for its stability at high temperatures, being safe to handle, and its special ability to react when exposed to corrosion environment. These inducements make it perfect for strengthening composite coatings [8]. Developing a more advanced corrosion-resistant steel member is now an important issue in the marine field. Surface engineering, especially by the use of protective coatings, has been considered as one of the most effective solutions for the problems related to corrosion in such severe environments. TiO_2 exists in three common polymorphs: anatase, rutile and amorphous. The two phases differ in atomic arrangement and surface characteristics that affect the behavior of the resulting coating. Anatase possesses a high surface energy and a small particle size distribution and thus is also suitable for the uniform dispersion and enhanced corrosion resistance [9]. Because of rutile as the most stable phase of TiO_2, the hardness and heat resistance are enhanced [10]. One of the features of amorphous TiO_2, besides the lack of long-range ordering, is different nucleation, which may influence coating morphology and mechanical properties differently [11].

It has been reported by many researchers that adding TiO_2 particles to the electroless Ni-P coatings leads to remarkable improvement of wear resistance, microhardness, and corrosion resistance. It was reported [12] that with the addition of TiO_2 the barrier property of Ni-P layer was enhanced by minimizing the diffusion paths for corrosive material. Similarly, Srivastwa et al. developed Ni-P-TiO_2 coatings [13] indicated that corrosion resistance of coatings was affected by particle size, distribution, and phase. it was found that the anatase phase TiO_2 can form compact and uniform coating compared to that of the rutile phase, contributing to enhanced corrosion resistance and excellent surface morphology. However, there is still a lack of knowledge concerning their relative behaviour in different structural forms of TiO_2 into the Ni-P matrix when exposed to a marine environment. Few systematic studies have investigated how anatase, rutile, and amorphous phases specifically contribute to the coating properties, such as surface roughness, coating thickness, roughness, and corrosion resistance, on the marine grade AH36 steel [14-16]. The differentiation between these are very important in order to optimise the coating process to individual high performance application for marine. The motivation of this work originates from the assumption that the form of TiO_2 can affect the dispersion, nucleation, and interfacial adherence of Ni-P matrix coatings and on their overall properties [17]. The superior behavior of anatase-based coatings arises from its high surface energy and fine crystallite size, which enhance nucleation and uniform Ni–P matrix formation. Rutile, being the most stable phase, provides good thermal stability but lower interfacial reactivity due to its coarser structure. Amorphous TiO_2 lacks atomic ordering, causing poor dispersion and higher surface roughness. Anatase facilitates better catalytic activity and compact passive film formation, improving corrosion resistance. Thus, the TiO_2 phase directly governs coating density, adhesion, and electrochemical protection efficiency [18–19].

The present work focuses on electroless plating of Ni-P composite coatings with varied polymorphic phases of TiO_2 i.e., anatase, rutile, and amorphous on marine-grade AH36 steel. For the first time, plant extracted TiO_2 nano particles are used in the electroless coating to develop corrosion resistance coating on the AH36 substrate. The schematic representation of the flow of this research work is given in the figure 2.

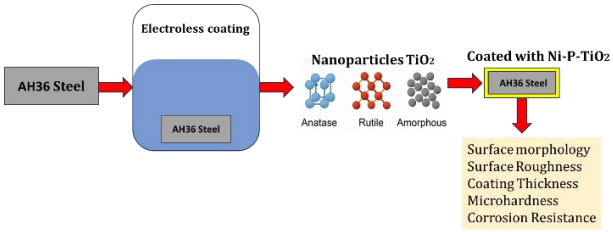

Fig. 2. Schematic representation of the flow of this research work.

It is intended to analyze how these various structures impact the microstructure, phase composition, mechanical hardness, surface roughness and corrosion resistance in the coatings. The objective is that the TiO_2 structure may influence the homogeneity of dispersion, nucleation behavior, and interfacial bonding in the Ni-P matrix, characteristic that affects the coating quality samples were tested with pure phases of TiO_2, such as anatase, rutile, amorphous, and TiO_2 mixed phase, a combination of the three mentioned phases in the composition of 0.05 grams of each. The coatings were analyzed for their characterization using SEM, AFM, XRD, microhardness, and electrochemical corrosion tests. These techniques provided a detailed characterization of the surface structure and the electrochemical properties.

2. EXPERIMENTAL DETAILS AND PROCEDURES

AH36 steel, sourced from the Indian Navy's reprocessing yard, is machined into the needed shapes and verified for the elemental composition as shown in the table 1.

Table 1. Elemental composition in percentage [6].

C	Mn	Ti	P	Si	Al	Cu	Cr	Fe
0.17	1.22	0.017	0.012	0.39	0.042	0.016	0.03	Remaining

Chemicals are sourced from the lab for preparing & treating surfaces (Table 2). Sulfuric acid is used to activate the substrate's surface, boosting its reactivity for coating. Acetone cleans off impurities like oils leaving a clean surface. Ethanol helps with degreasing so that the coating sticks better by getting rid of organic matters. The nitric acid is utilized to clean beakers and other glassware.

Table 2. Chemicals required for pre-treatment process.

S.No	Required chemicals	Purpose
1	Sulfuric acid	To activate the surface
2	Acetone	To remove the impurities
3	Ethanol	Degreasing the substrate
4	Nitric Acid	For cleaning the beakers

To set up the electroless Ni-P-TiO_2 coating bath, certain chemicals are acquired to ensure controlled deposition & quality deposit (see Table 3). Sodium hypophosphite (40 g) acts as the main reducing agent, letting nickel deposit on the substrate without the aid of an external current. Sodium tri-citrate (50 g) works as a complexing agent, keeping metal ions steady in the solution & stopping unwanted reactions. Ammonium chloride (50 g) keeps things balanced & conductive. Liquid ammonia tunes the pH level key for regulating speed of the reaction. Nickel sulphate (30 g) provides nickel ions for forming a smooth Ni-P matrix during coating. All reagents used for the preparation of electrolyte and pre-treatment process in this study were purchased from Merck with a stated purity of 99.9%.

Table 3. Chemicals required for the preparation of electrolyte.

S.No	Required chemicals to be purchased	Quantity	Purpose
1	Sodium hypophosphite	40 gm	Reducing agent
2	Sodium tri-citrate	50 gm	Complexing agent
3	Ammonium chloride	50 gm	Regulator
4	Liquid ammonia	required	pH
5	Nickel Sulphate	30 gm	Ni source

2.1 Synthesis of TiO_2 nanoparticles using plant extract

TiO_2 nanoparticles were synthesized through an inexpensive green synthesis method utilizing the extract of Indigofera tinctoria (true indigo), which serves as both a reducing and capping agent [20]. The extract is added dropwise to a 100 mL beaker containing titanium tetra-isopropoxide (TIP). The solution was agitated at ambient temperature until its color transformed from pristine white to a yellowish-grey. The alteration in colour serves as an indication of the synthesis of TiO_2 nanoparticles. Subsequently, the solution underwent a filtration process and was subjected to drying at a temperature of 110 °C. The dried sample underwent calcination in a muffle furnace at 500 °C to facilitate the formation of the anatase phase, followed by a subsequent calcination at 800 °C to achieve the rutile phase of the as synthesized nanoparticles [21]. The process for developing the nano particles are provided in the figure 3.

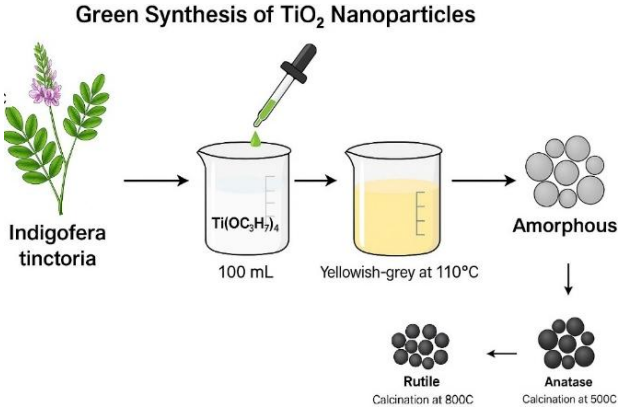

Fig. 3. Schematics representation of synthesis of TiO_2 nanoparticles.

The coatings' thickness of electroless Ni-P-TiO_2 was estimated for all four of the specimens as depicted in the figure 8. The sample 3 which is prepared using the anatase TiO_2 (0.1 g) shows the largest coating thickness (about 27 µm) because of the high surface reactivity and uniform coverage of the anatase phase, making continuous autocatalytic deposition to be achieved. The sample 1 (rutile TiO_2, 0.1 g) showed relatively close (up to 24 µm); it could have good deposition characteristics with 24 like due to crystalline stability of rutile. Sample 2 (amorphous TiO_2, 0.1 g) exhibited lower coating thickness of 20 µm because of amorphous character resulting in reduced nucleation and growth during coating. The mixed phase hybrid structure (0.05 g each of rutile, amorphous and anatase) exhibited the least thickness (16 µm), which can be attributed to interferences introduced by phases, improper dispersion of particles and decreased catalytic activity. In general, anatase-modified formulations resulted in higher coating thickness.

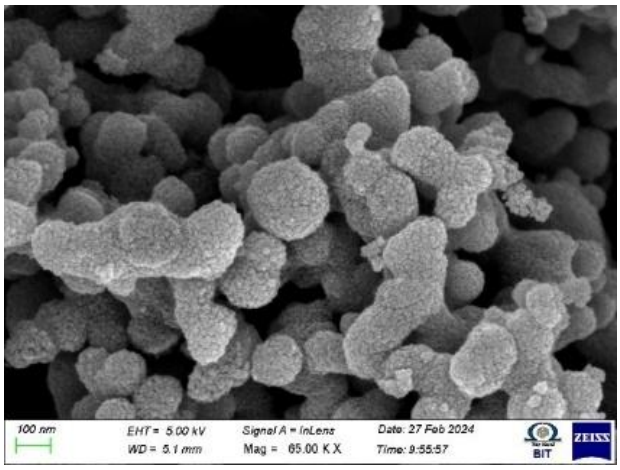

(a)

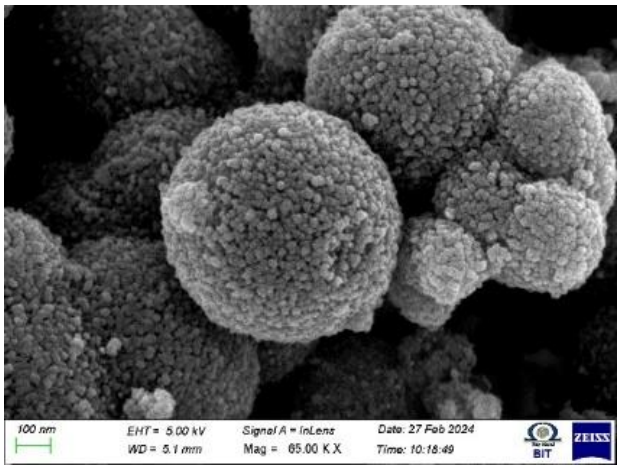

(b)

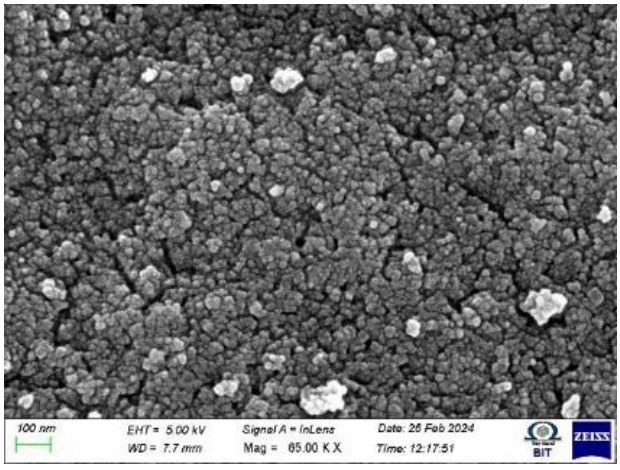

(c)

Fig. 4. SEM images of TiO_2 (a) Anatase, (b) Rutile, (c) Amorphous.

TiO_2 nanoparticles were made in three phases & checked using SEM as shown in the figure 4. XRD analysis was done to spot TiO_2 crystal forms inside the electroless Ni-P deposit. Patterns confirmed different TiO_2 polymorphs anatase, rutile, and amorphous in samples. Anatase TiO_2 samples had sharp peaks at distinctive 2θ values like 25.3°, 37.8°, and 48.0°, linked to (101), (004), and (200) planes, showing high crystallinity. Rutile samples showed strong peaks near 27.4°, 36.1°, and 54.3°, linked to (110), (101), and (211) planes, confirming their crystalline rutile structure. In comparison, amorphous TiO_2 samples had broad, weak peaks, indicating low crystallinity as shown in the figure 5.

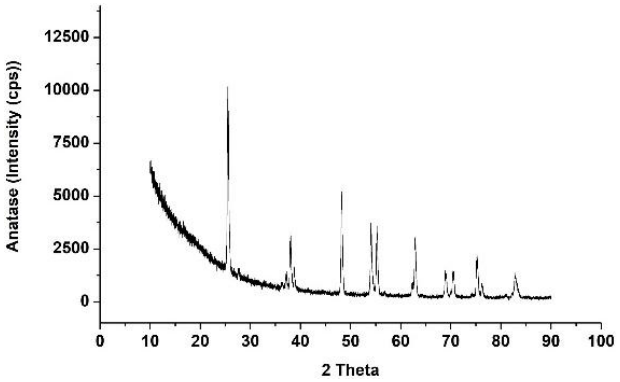

(a)

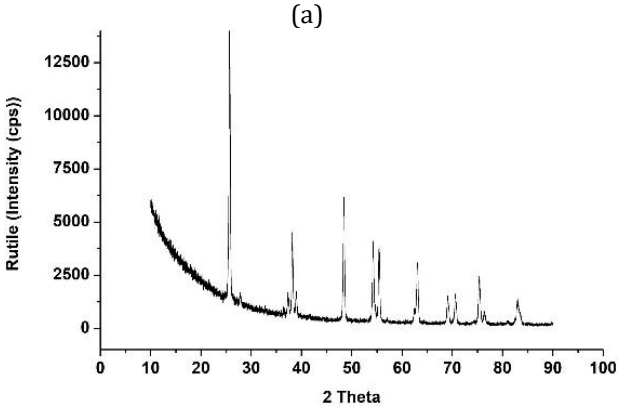

(b)

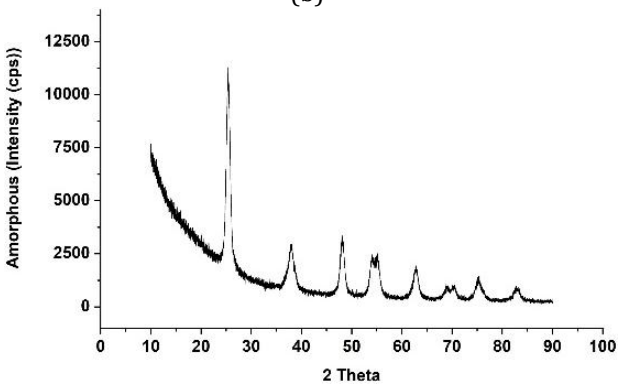

(c)

Fig. 5. X-ray diffractogram of various phases of TiO_2 particles.

Glassware and laboratory apparatus is needed to conduct the electroless coating operation in an efficient and safe manner. A conical flask is employed to mix and prepare chemical solutions, and a measuring jar aids in the precise

measurement of volumes. Four nos 250 mL beakers are available to contain, blend, or heat solutions at different points in the procedure. A temperature-controlled water or oil bath is used to keep the bath at the desired temperature as shown in the figure 6.

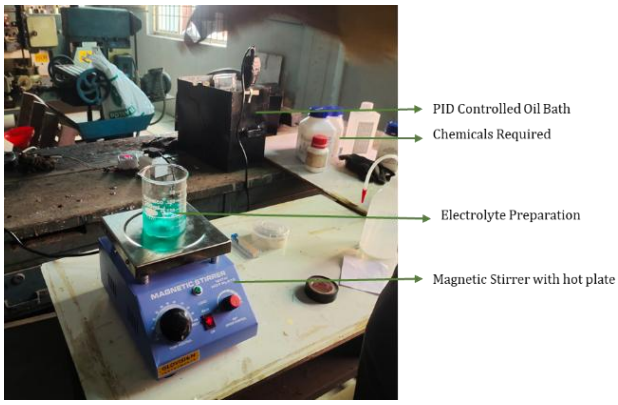

Fig. 6. Experimental setup.

In terms of watching temperature, a thermometer is required. For keeping free from pollution and protecting the chemicals, air-tight containers (5 units) are used. Hand gloves (2 pair) also packet of tissue paper is needed for cleanliness and safety precaution during handling. A hot plate with magnetic stirrer is used to homogenize and regulate the temperature of the bath. For liquid transfer without spillage, we use a small size glass funnel (1 unit). pH indicator is an indispensable tool for observing and regulating the pH of the bath. It is also necessary to use a pipette (1 unit) to add of small amount of ammonia whenever required. For surface cleaning small roll of cotton is utilized (1 unit). Glass rod (1 unit) to help with the manual mixing of a solution during preparation or chemical transfer. The composition of the deposit on the samples are listed in the table 4.

The electroless coatings were deposited in a 250 mL glass beaker at 85°C for 1 h. The Zwitterionic surfactant was weighed to 0.018 g and dissolved in 1L of distilled water. It was then mixed thoroughly by a magnetic stirrer. Prepared surfactant (5 drops) was added in the electrolyte after reaction starts. While depositing particles the electrolyte was magnetically stirred to keep the particle in suspension. The visual comparison of samples before coating, after pretreatment, and after electroless coating is presented in Figure 7, illustrating the progressive surface transformation during each stage of processing.

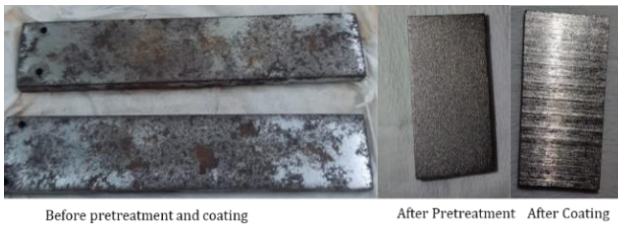

Fig. 7. Before and after coating of the samples.

Table 4. Composition of the samples developed using electroless coating process

Description	Composition
Sample 1	Ni-P- TiO_2 (Rutile 0.1g)
Sample 2	Ni-P- TiO_2 (amorphous 0.1g)
Sample 3	Ni-P- TiO_2 (Anatase 0.1g)
Sample 4	Ni-P- TiO_2 (Rutile 0.05g + amorphous 0.05g + Anatase 0.05g) Hybrid

The coating duration for all substrates was fixed at 1 hours. The coating thickness was calculated using the weight gain method, as described by Eq. (1)

$$T = \frac{WX10^4}{dAt} \quad (1)$$

where T is the deposition rate (μm/h), W is the weight gain of the sample (g), d is the density of the coating (g/cm^3), A is the surface area of the substrate (cm^2), and t is the immersion time in the electrolyte bath. The coatings surface morphology was assessed using a SEM, specifically the Hitachi Model S-3400N, operated at an accelerating voltage of 15 kV. Elemental analysis of the deposits was conducted with an attached EDS system. Phases and structures were identified using XRD with a Rigaku Ultima IV diffractometer featuring a copper anode. The XRD patterns were documented over a 2θ range from 10° to 90°, with a step size of 0.02° per second. The surface texture and roughness were examined through AFM using a Bruker Dimension Icon system functioning in tapping mode, with scans covering a 5 × 5 μm^2 area. The coated substrates underwent degreasing with acetone, were thoroughly rinsed with deionized water, and then air-dried. Corrosion properties were assessed in an electrolyte solution with 3.5 wt. % sodium chloride. The surface area of the working electrode (substrate) was kept at 1 cm^2. A graphite rod was used as the counter electrode, and a saturated calomel electrode (SCE) served as the reference. Initially, open-circuit potential (OCP) measurements were taken, followed by potentiodynamic polarization at a scan rate of 1

mV/s. The samples were submerged in the electrolyte for 30 minutes before polarization to stabilize OCP. Current and potential were tracked simultaneously, and the data collected were utilized to generate Tafel plots for corrosion analysis.

3. RESULTS AND DISCUSSIONS

To study the effect of the phase composition of TiO_2 particles on the coating performance, four types of Ni-P-TiO_2 composites were deposited, which were prepared by different types of TiO_2 nanoparticles. Sample 1 was included with 0.1 g of rutile-phase TiO_2 having a high refractive index and thermal stability. Sample 2 contained 0.1 g of amorphous TiO_2, which has no long-range order and is anticipated to nucleate and disperse differently. Sample 3 included 0.1 g of anatase-phase TiO_2 which is a metastable crystalline phase whose high surface activity and well-dispersed fine particles could, in some instances, lead to a better coated layer. Sample 4 was prepared as a composite material comprising an equal ratio (0.05 of each phase, rutile, amorphous and anatase) to examine the interfering or synergistic interaction of the mixture phase in the Ni-P matrix. This phase became the goal to study the effect of TiO_2 structure on the morphology, the hardness, the corrosion resistance, and the quality of coating.

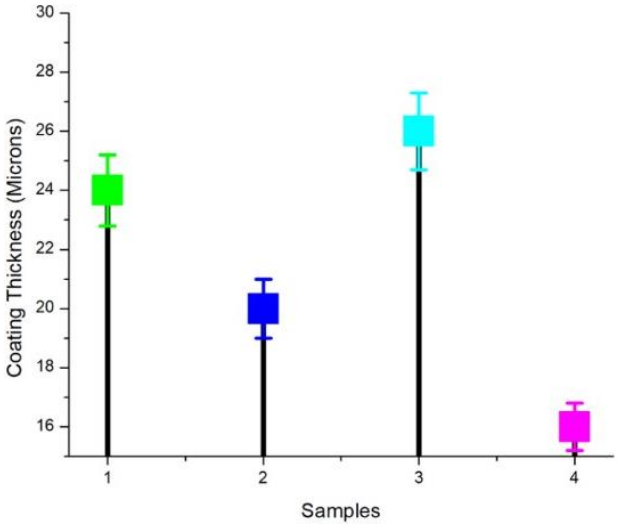

Fig. 8. Coating thickness of the deposits.

The difference in the thickness of coating obtained between the present work and work carried out in last decade on electroless Ni–P–TiO_2 composite is closely related to standard coatings deposited also under the same conditions routinely yield thicknesses of 10–15μm [22], whereas for processes that have been optimized and which involve the use of surfactants, average thickness values around 30μm are reported [23]. In contrast, the anatase-based coatings produced herein possess thicknesses of up to about 27μm, which lies closer to the higher end of the published range and which is in excess of values realized under non-optimized conditions. These findings support the premise that precise control of bath composition especially with surfactant species and fine TiO_2 particles significantly promotes nucleation and accelerates the autocatalytic growth rate, such that thicker, more uniform films are obtained.

Four Ni-P-TiO_2 coated samples exhibit distinguishable surface structures under SEM observation as shown in the figure 9. In the case of sample S1 (rutile TiO_2) the surface is apparently featureless and linear in appearance with few particles lying on it, thus, insinuating low TiO_2 contribution and homogeneous deposition of Ni-P. On the other hand, S2 (amorphous TiO_2) has a rougher surface seen to be densely filled with spherically shaped nodules indicating an improved number of nucleation sites but probably agglomerates due to low crystallinity. Sample S3 (anatase TiO_2) shows a homogeneous distribution of small, semi-spherical particles, which correspond to well-dispersed anatase particles that contribute to produce uniform deposit and surface growth. This morphology is related to thicker coatings and better properties. Sample S4, a combination of all three TiO_2 structures, displays an inconclusive, nonuniform surface, some fine and some coarse nodules, suggesting uncontrolled precipitation through incompatible phase interactions. In general, anatase-based sample (S3) showed the best microstructure for dense and uniform coatings with the best particles distribution among others, and the morphological inhomogeneity was introduced by the hybrid one in S4. Birla et al. [23] reported even higher resolution particle-level morphology of nanoparticulate coatings where electroless Ni growth resulted in homogeneous 1–2nm thick Ni coatings over anatase TiO_2 cores, albeit with emphasis on photocatalytic rather than bulk film properties [24,25].

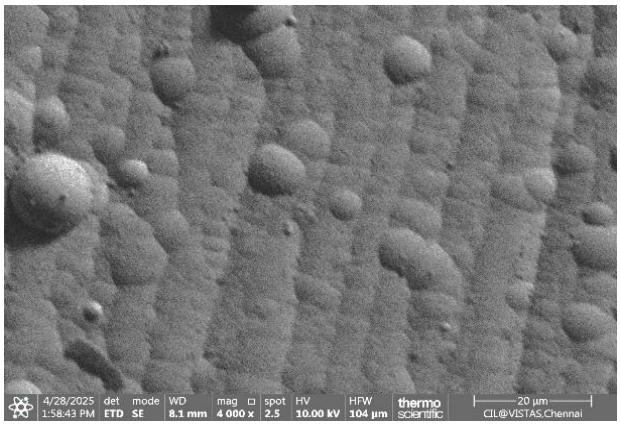

(a)

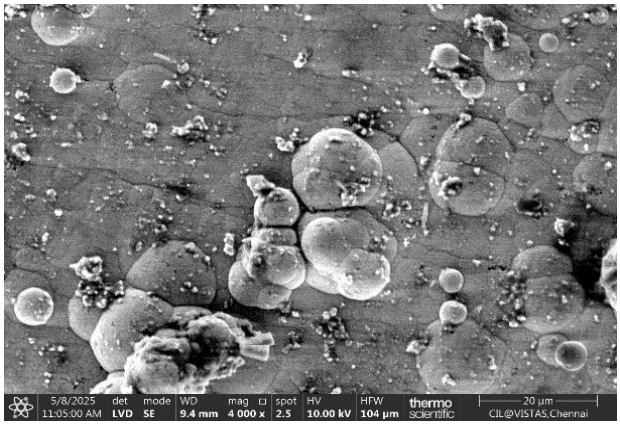

(b)

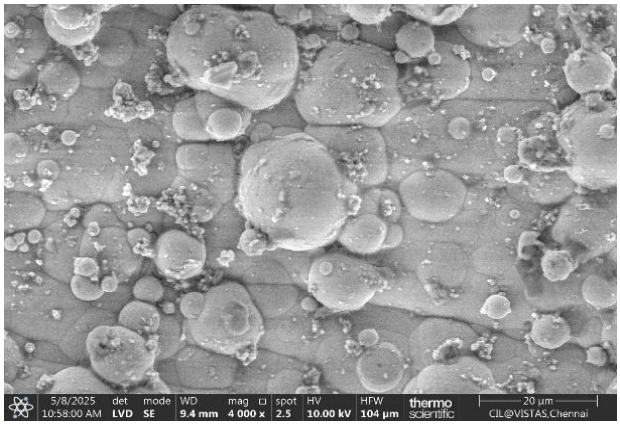

(c)

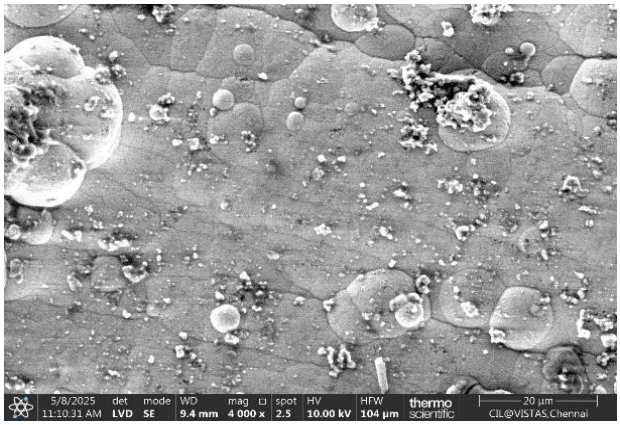

(d)

Fig. 9. Surface morphology of the prepared samples.

Contrarily, with respect to the composites' surface morphology reviews under surgical-grade Ni–P–TiO_2 coatings, the inclusion of surfactants and nanoscale TiO_2 give rise to compact, nodular structures that benefit tribological behavior [26].

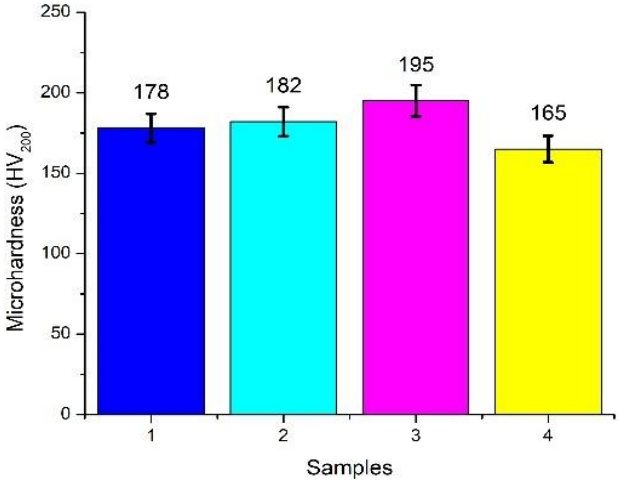

Fig. 10. Microhardness value of the deposits.

The microhardness of the Ni-P-TiO_2 coated electroless samples was measured with a Vickers indenter of 200 g load (HV200) is shown in the figure 10. As per ASTM E384 standard, five measurements were taken for each sample, and their average was recorded as the microhardness value. The findings showed a significant difference in the hardness for different phases of TiO_2. The microhardness of sample 3was highest with the value close to 200 HV, and this is mainly due to its fine grains and more uniformly dispersion, which can effectively improve mechanical strength of the coating. Sample 2 also exhibited high hardness of a level near that of Sample 3, indicating that the amorphous phase was densified in spite of the lower crystallinity. Sample 2 had a medium hardness, on the other hand, sample 4 (combination of 0.05 g of each TiO_2 phase) had the lowest microhardness out of all of the samples tested. This decrease could be attributed to non-uniform particle dispersion and diminished crystallinity balance. Altogether, the anatase phase greatly improved coating hardness and was considered more feasible. The results of this study are consistent with recent work in the area of electroless Ni–P–TiO_2 composite research both in microhardness measurements and corrosion behavior. The through incorporation of TiO_2 nanoparticles increased microhardness value is much higher; other works have also reported such enhancements; for example, microhardness values as high as 1124 HV for the coatings annealed at 400

°C [27]. Similarly, Gadhari and Sahoo [26] observed that higher content of the incorporated TiO_2 and optimized annealing conditions provide higher hardness and better corrosion protection (less corrosion current density and higher charge transfer resistance) for Ni–P–TiO_2 composites.

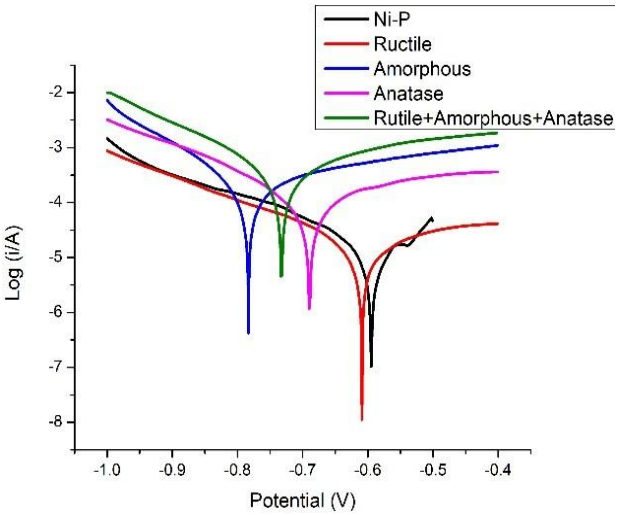

Fig. 11. Corrosion analysis of the samples using Tafel plot.

Corrosion performance of samples with diverse TiO_2 phases in the Ni-P-TiO_2 film were evaluated using Tafel polarization curves analysis is shown in the figure 11. The differences in corrosion potential (Ecorr) and current density (Icorr) can be seen from the curves, which are the indicative parameters regarding the corrosion resistance. The sample 1 (rutile 0.1 g) showed the moderate corrosion potential ca −0.73 V with the current density indicating the fair resistance. The current density of sample 2 (amorphous 0.1 g) was the lowest, and a more negative potential at –0.80 V, indicating better passive film formation ability as well as stronger corrosion resistance. Sample 3 (anatase 0.1 g) exhibited the best corrosion resistance with the most positive Ecorr (around –0.65 V) and the lowest Icorr due to better dispersion of particles and higher degree of coating uniformity. Sample 3 (a mixture of TiO_2 phases) had the least corrosion resistance, while sample 4 (hybrid TiO_2 phases) showed moderate corrosion resistance. In general, sample 3 (anatase) exhibited the best electrochemical performance, which was consistent with its relatively smooth surface, developed here indicating that surface morphology plays a key role in the corrosion process. Tafel plots for our anatase coats exhibit a significant noble shift in corrosion potential and lower current density of corrosion when compared to the pure Ni–P coated samples, a trend similar to those reported for the microwave-annealed Ni–P–TiO_2 sample previously [28].

AFM measurements were also conducted for Ni-P-TiO_2-coated samples with varying TiO_2 phases to determine the surface morphology and roughness as shown in the figure 12. A polarity Type 1 material sample with rutile TiO_2 (0.1 g) had a roughness (Ra) of 106.6 nm suggesting some degree of roughness. Sample 2, whose TiO_2 is of amorphous shape (0.1 g), exhibited the highest Ra of 170.1 nm and the surface was prominent in groove and the dispersion of particle was poor. Sample 3 (anatase TiO_2 0.1 g) was found to have the minimum roughness (67.4 nm) and it had a smooth and well distributed surface, which indicated a better integration and coating quality of the particles. Hybrid Sample 4 with equal amounts of rutile, amorphous, and anatase phases (0.05 g of each) showed a Ra of 85.05 nm which suggested a balanced surface texture because of synergistic particle interaction. Sample 3 had better surface properties than all, and Sample 2 possessed relatively rough surface. The findings emphasize the importance of TiO_2 morphology with respect to film uniformity and quality.

The AFM results in this study for Ni–P–TiO_2 coatings shows higher surface roughness as compared to pure Ni–P coatings. In particular, the RMS roughness (R_{pms}) increases from ~7 nm (pure Ni–P) to ~33 nm with 2 g/L TiC addition simultaneously analogous with observations when ceramic powders are added [28]. This is consistent with atomic-layer-deposited TiO_2 films on Ti substrates, where the RMS roughness increased from ~13nm to ~40nm after anatase crystallization. In the same way, sol–gel-coated TiO_2 glass substrates had very low, ultra-flat roughness values particularly ~0.86nm and demonstrated how AFM-observed topography is dependent on deposition method and underly substrate [28]. Our results suggest that the addition of TiO_2 to the electroless Ni–P background introduces nano-morphology in the form of nano-texturing and higher roughness (~30–40nm) consistent with both composite and thin-film distribution observations. This increase roughness should have a more beneficial effect for mechanical interlocking and coating adhesion, which are the most important properties for tribo-corrosion and wear

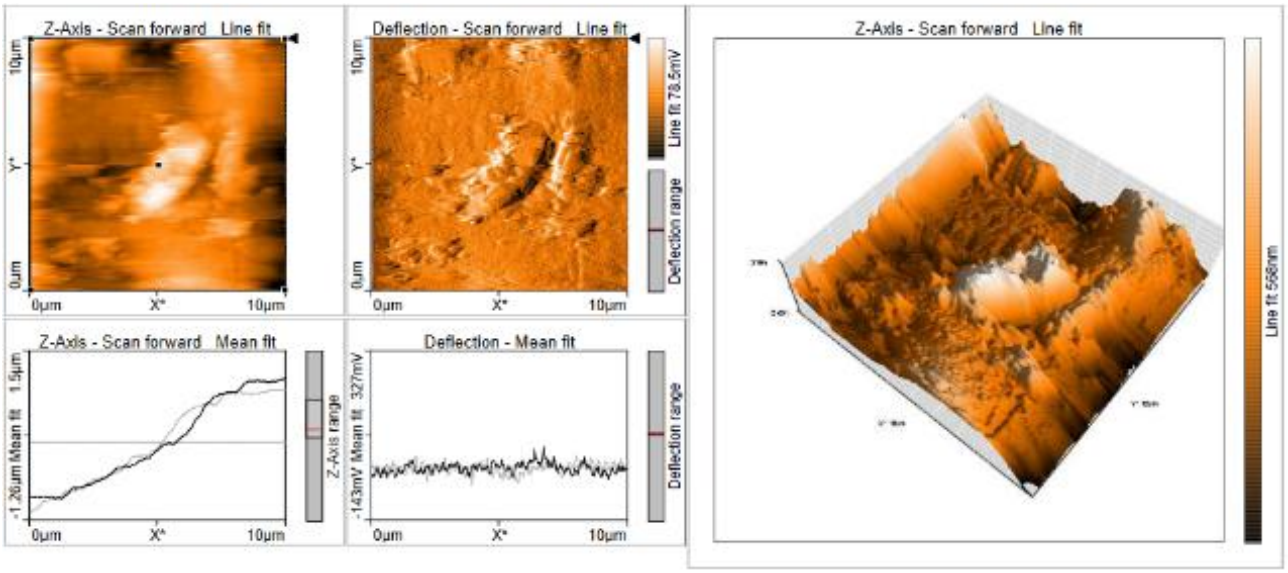
Z-Axis - Scan forward Line fit
Deflection - Scan forward Line fit
Z-Axis - Scan forward Line fit
Z-Axis - Scan forward Mean fit
Deflection - Mean fit
Line fit 78.5mV
Deflection range
Line fit 568nm
Z-Axis range
0µm
10µm
X*
Y*

(a)

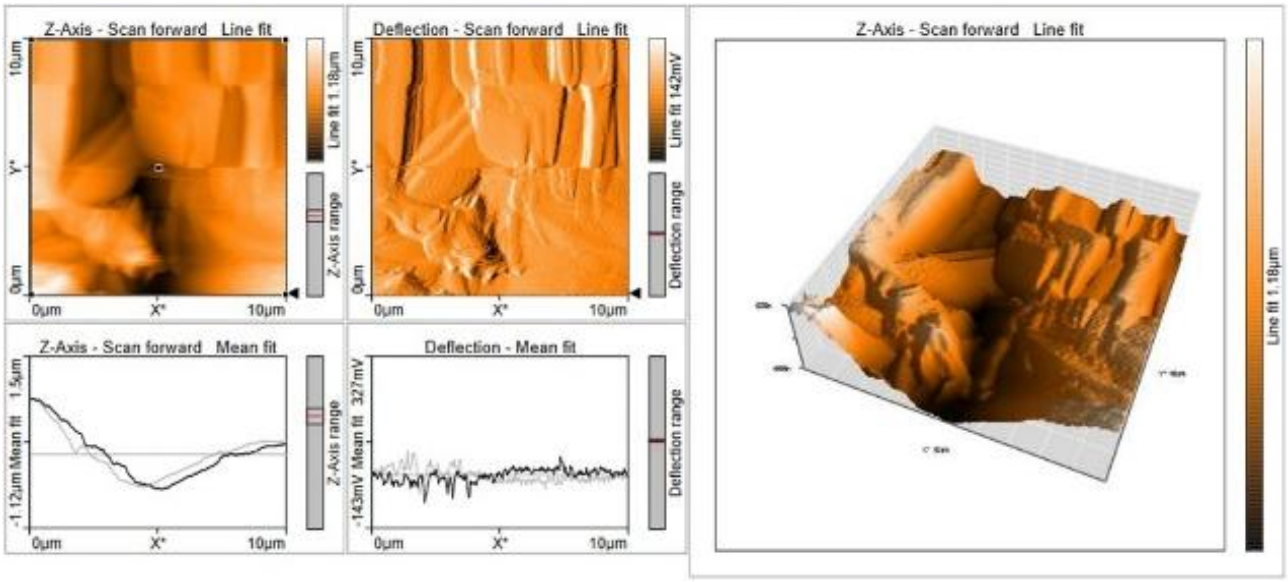
Z-Axis - Scan forward Line fit
Deflection - Scan forward Line fit
Z-Axis - Scan forward Line fit
Z-Axis - Scan forward Mean fit
Deflection - Mean fit
Line fit 1.18µm
Line fit 142mV
Deflection range
Z-Axis range
0µm
10µm
X*
Y*

(b)

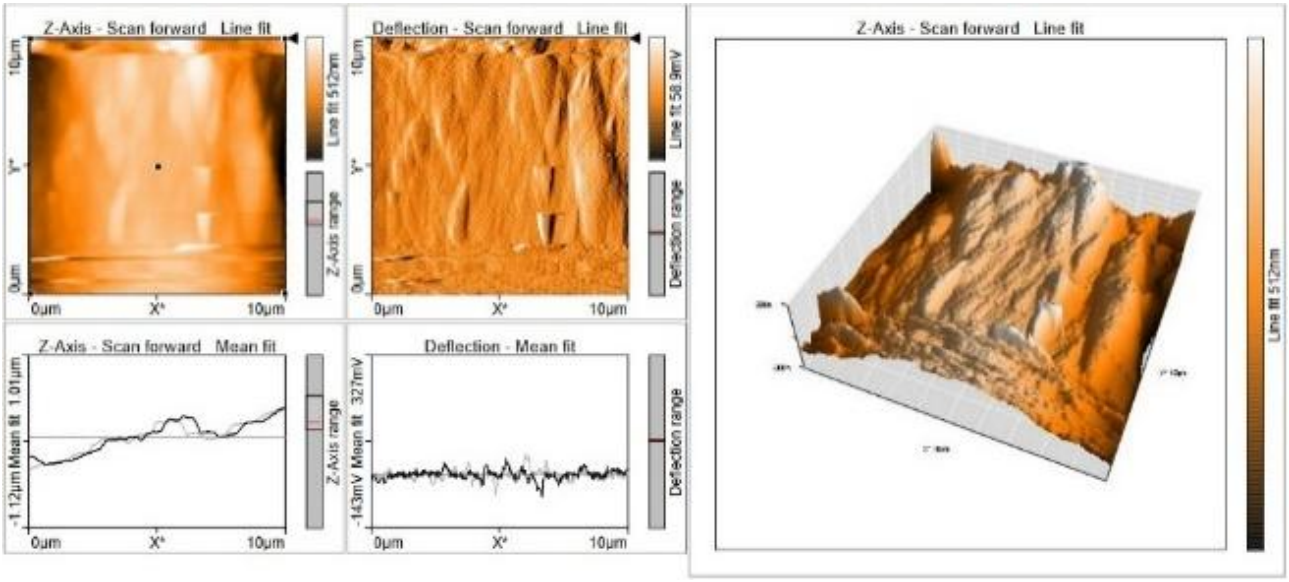
Z-Axis - Scan forward Line fit
Deflection - Scan forward Line fit
Z-Axis - Scan forward Line fit
Z-Axis - Scan forward Mean fit
Deflection - Mean fit
Line fit 512nm
Line fit 58.9mV
Deflection range
Z-Axis range
0µm
10µm
X*
Y*

(c)

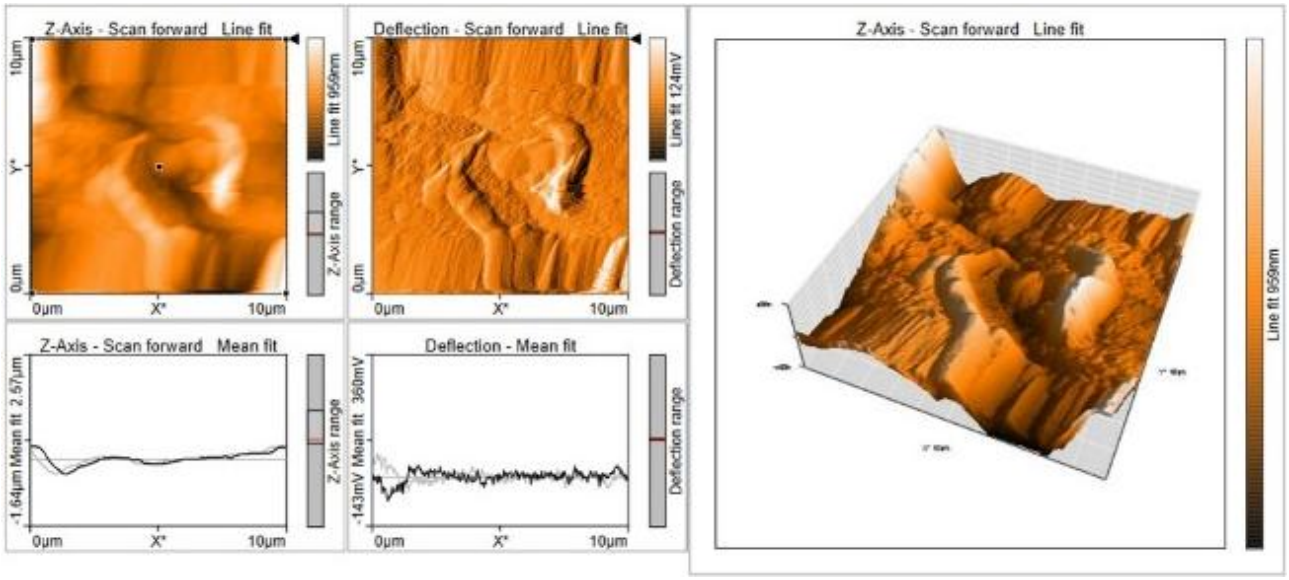

(d)

Fig. 12. Surface topography of the surface of the deposits.

The analysis from coating thickness, surface morphology (SEM and AFM), microhardness, and corrosion behavior (Tafel polarization) reveals a clear correlation between structural modifications and improved corrosion resistance of the Ni–P–TiO_2 composite coatings. The measured coating thickness (27 µm) contributes significantly to the barrier properties by providing uniform coverage and mitigating electrolyte penetration. SEM micrographs revealed a dense, nodular surface morphology with fine TiO_2 dispersions, while AFM analysis confirmed an increase in surface roughness, indicative of a textured surface that enhances mechanical interlocking and adhesion. These morphological characteristics are consistent with previous studies reporting that nanostructured roughness enhances both coating integrity and electrochemical stability by minimizing defect pathway. Comparable findings have been reported for Ni–P–ZrO_2 and Ni–P–TiC systems, where increased hardness correlated with improved corrosion resistance due to reduced susceptibility to crack initiation and propagation. Electrochemical corrosion tests using Tafel polarization confirmed the superior corrosion resistance of the TiO_2-modified coatings, as evidenced by a more positive corrosion potential and a marked decrease in corrosion current density. These improvements are consistent with literature where the incorporation of TiO_2 into Ni–P matrices led to the formation of stable passive films, increased charge transfer resistance, and suppression of micro-galvanic cells. The increase in surface roughness and coating thickness contributes to improved microhardness, which in turn enhances the physical and chemical stability of the passive layer. This multilayered improvement ultimately results in significantly better corrosion resistance, establishing the Ni–P–TiO_2 nanocomposite coating as a promising candidate for applications requiring both mechanical durability and electrochemical protection.

4. CONCLUSIONS

The present study effectively revealed the synthesis and characterization of electroless Ni–P–TiO_2 composite coatings with varying polymorphic forms of TiO_2, i.e., anatase, rutile, amorphous, and hybrid blend, over AH36 marine-grade steel substrates. The addition of TiO_2 particles had a marked effect on the microstructure, coating thickness, surface roughness, microhardness, and corrosion resistance of the coatings.

Among all the samples, the Ni–P–TiO_2 coating reinforced with the anatase phase exhibited superior performance. It showed the maximum coating thickness (27 µm), indicating good deposition efficiency, and displayed a uniform, compact surface morphology with well-dispersed nodular features, as verified by SEM observations. The anatase sample had the lowest

surface roughness (67.4 nm) with better surface homogeneity, resulting in higher electrochemical stability. The microhardness tests indicated that the anatase-reinforced coating (approximately 200 HV) possessed the maximum hardness due to the dense interfacial bonding between ceramic particles and the Ni–P matrix.

The anatase-modified coating also demonstrated the best corrosion resistance. According to Tafel polarization analysis, it exhibited the most positive corrosion potential and the lowest corrosion current density among the four specimens. In contrast, coatings with rutile and amorphous TiO_2 phases showed moderate enhancement. The amorphous TiO_2 sample displayed higher roughness and a thinner coating film, attributed to random particle distribution and a lower degree of crystallinity.

The results indicate a 13.5% increase in performance compared with the Ni–P sample, 67.4 nm surface roughness, and 200 HV (25% increase) microhardness. The findings explicitly demonstrate that the anatase phase provides the best coating quality and corrosion protection for AH36 steel in marine environments. These results offer valuable insight for the optimal selection of TiO_2 phases in electroless composite coatings and serve as a reference for advancing surface engineering in marine applications. Further studies may focus on long-term corrosion exposure evaluations, thermal stability testing, and optimization of hybrid reinforcement methods to further enhance coating performance for marine and offshore engineering applications.

REFERENCES

[1] V. Krishnakumar and R. Elansezhian, "Wear and corrosion behavior of electroless Ni-P- TiO2-Al2O3 nanocomposite coatings on magnesium AZ91D alloy," *IOP Conference Series Materials Science and Engineering*, vol. 912, no. 5, p. 052020, Aug. 2020, doi: 10.1088/1757-899x/912/5/052020.

[2] W. Zhang *et al.*, "Microstructure and properties of duplex Ni-P-TIO2/NI-P nanocomposite coatings," *Materials Research*, vol. 22, no. suppl 2, Jan. 2019, doi: 10.1590/1980-5373-mr-2018-0748.

[3] Z. Karaguiozova, J. Kaleicheva, V. Mishev, and G. Nikolcheva, "Enhancement in the tribological and mechanical properties of electroless Nickel-Nanodiamond coatings plated on iron," *Tribology in Industry*, vol. 39, no. 4, pp. 444–451, Dec. 2017, doi: 10.24874/ti.2017.39.04.03.

[4] K. Shahzad *et al.*, "Corrosion and heat treatment study of electroless NIP-TI nanocomposite coatings deposited on HSLA Steel," *Nanomaterials*, vol. 10, no. 10, p. 1932, Sep. 2020, doi: 10.3390/nano10101932.

[5] I. A. Shozib *et al.*, "Modelling and optimization of microhardness of electroless Ni–P–TiO2 composite coating based on machine learning approaches and RSM," *Journal of Materials Research and Technology*, vol. 12, pp. 1010–1025, Mar. 2021, doi: 10.1016/j.jmrt.2021.03.063.

[6] R. A. S. Selvan, D. G. Thakur, M. Seeman, and M. Naik, "Surface modification of AH36 steel using ENI-P-NaNO TIO2 composite coatings through ANN-Based modelling and prediction," *Journal of Marine Science and Application*, vol. 21, no. 3, pp. 193–203, Sep. 2022, doi: 10.1007/s11804-022-00288-5.

[7] Z. Hao *et al.*, "Progress of material degradation: metals and polymers in deep-sea environments," *Corrosion Reviews*, vol. 43, no. 3, pp. 315–334, Dec. 2024, doi: 10.1515/corrrev-2024-0009.

[8] J. D, A. Ziout, and J. A. Qudeiri, "Optimization of P-GMAW parameters using Grey relational analysis and Taguchi method," in *2021 IEEE 12th International Conference on Mechanical and Intelligent Manufacturing Technologies (ICMIMT)*, Cape Town, South Africa: IEEE, May 2021, pp. 191–196. doi: 10.1109/ICMIMT52186.2021.9476176.

[9] M. Zhu, Y. Chen, Y. Chen, and K. Hu, "Application of Taguchi-grey relational analysis for optimizing process parameters of laser cladding for 316L stainless steel," *International Journal on Interactive Design and Manufacturing (IJIDeM)*, vol. 19, no. 9, pp. 6417–6428, Jan. 2025, doi: 10.1007/s12008-024-02218-x.

[10] M. Vijayanand, R. Varahamoorthi, P. Kumaradhas, S. Sivamani, and M. V. Kulkarni, "Regression-BPNN modelling of surfactant concentration effects in electroless Ni B coating and optimization using genetic algorithm," *Surface and Coatings Technology*, vol. 409, p. 126878, Jan. 2021, doi: 10.1016/j.surfcoat.2021.126878.

[11] A. Salicio-Paz, I. Ugarte, J. Sort, E. Pellicer, and E. García-Lecina, "Full optimization of an electroless nickel solution: boosting the performance of Low-Phosphorous coatings," *Materials*, vol. 14, no. 6, p. 1501, Mar. 2021, doi: 10.3390/ma14061501.

[12] S. Sarkar, R. K. Baranwal, R. Nandi, M. G. Dastidar, J. De, and G. Majumdar, "Parametric optimization of surface roughness of electroless NI-P coating," in *Lecture notes on multidisciplinary industrial engineering*, 2020, pp. 197–207, doi: 10.1007/978-981-15-4550-4_12.

[13] A. K. Srivastwa, S. Sarkar, J. De, and G. Majumdar, "Parametric optimization of electroless Ni-P-CNT coating using genetic algorithm to maximize the rate of deposition," *Materials Today Proceedings*, vol. 66, pp. 3769–3774, Jan. 2022, doi: 10.1016/j.matpr.2022.06.106.

[14] H. Nazari, G. B. Darband, and R. Arefinia, "A review on electroless Ni–P nanocomposite coatings: effect of hard, soft, and synergistic nanoparticles," *Journal of Materials Science*, vol. 58, no. 10, pp. 4292–4358, Feb. 2023, doi: 10.1007/s10853-023-08281-1.

[15] E. M. Fayyad, A. M. Abdullah, M. K. Hassan, A. M. Mohamed, G. Jarjoura, and Z. Farhat, "Recent advances in electroless-plated Ni-P and its composites for erosion and corrosion applications: a review," *Emergent Materials*, vol. 1, no. 1–2, pp. 3–24, Jun. 2018, doi: 10.1007/s42247-018-0010-4.

[16] S. A. Abde. L. Gawad, A. M. Baraka, Morsi, and A. Eltoum, "Development of Electroless Ni-P-Al2O3 and Ni-P-TiO2 Composite Coatings from Alkaline Hypophosphite Gluconate Baths and their Properties," *International Journal of Electrochemical Science*, vol. 8, no. 2, pp. 1722–1734, Feb. 2013, doi: 10.1016/s1452-3981(23)14260-x.

[17] R. Muraliraja *et al.*, "A review of electroless coatings on non-metals: Bath conditions, properties and applications," *Journal of Alloys and Compounds*, vol. 960, p. 170723, May 2023, doi: 10.1016/j.jallcom.2023.170723.

[18] F. Ali, M. Waseem, R. Khurshid, and A. Afzal, "TiO2 reinforced high-performance epoxy-co-polyamide composite coatings," *Progress in Organic Coatings*, vol. 146, p. 105726, May 2020, doi: 10.1016/j.porgcoat.2020.105726.

[19] H. Zhang, J. Zou, N. Lin, and B. Tang, "Review on electroless plating Ni–P coatings for improving surface performance of steel," *Surface Review and Letters*, vol. 21, no. 04, p. 1430002, Mar. 2014, doi: 10.1142/s0218625x14300020.

[20] M. Aravind, M. Amalanathan, and M. S. M. Mary, "Synthesis of TiO2 nanoparticles by chemical and green synthesis methods and their multifaceted properties," *SN Applied Sciences*, vol. 3, no. 4, Mar. 2021, doi: 10.1007/s42452-021-04281-5.

[21] W. Chen, W. Gao, and Y. He, "A novel electroless plating of Ni–P–TiO2 nano-composite coatings," *Surface and Coatings Technology*, vol. 204, no. 15, pp. 2493–2498, Feb. 2010, doi: 10.1016/j.surfcoat.2010.01.032.

[22] R. A. S. Selvan, D. G. Thakur, M. Seeman, R. Muraliraja, and Mohd. I. Ansari, "Modelling and optimisation of ENi-P-TiO2 coatings synthesised with Zwitterionic surfactant on naval grade AH36 Steel," *Sadhana*, vol. 47, no. 3, Jun. 2022, doi: 10.1007/s12046-022-01890-7.

[23] P. N. Birla *et al.*, "Electroless Ni plated nanostructured TiO2 as a photocatalyst for solar hydrogen production," *RSC Advances*, vol. 13, no. 29, pp. 20068–20080, Jan. 2023, doi: 10.1039/d3ra03139j.

[24] S. Amjad-Iranagh and M. Zarif, "TiO2 nano-particle effect on the chemical and physical properties of Ni-P-TiO2 nanocomposite electroless coatings," *Journal of Nanostructures*, vol. 10, no. 2, pp. 415–423, Apr. 2020, doi: 10.22052/jns.2020.02.019.

[25] P. Gadhari and P. Sahoo, "Effect of TiO2 particles on micro-hardness, corrosion, wear and friction of Ni–P–TiO2 composite coatings at different annealing temperatures," *Surface Review and Letters*, vol. 23, no. 01, p. 1550082, Aug. 2015, doi: 10.1142/s0218625x15500821.

[26] P. Gadhari and P. Sahoo, "Study of hardness and corrosion resistance of electroless NI-P-TIO2 composite coatings," *International Journal of Surface Engineering and Interdisciplinary Materials Science*, vol. 3, no. 2, pp. 18–40, Jul. 2015, doi: 10.4018/ijseims.2015070102.

[27] O. Fayyaz *et al.*, "Enhancement of mechanical and corrosion resistance properties of electrodeposited Ni–P–TiC composite coatings," *Scientific Reports*, vol. 11, no. 1, p. 5327, Mar. 2021, doi: 10.1038/s41598-021-84716-6.

[28] M. F. Achoi, M. N. Asiah, M. Rusop, and S. Abdullah, "Atomic Force Microscope (AFM) Studies of TiO2 Nanocoated Glass Surface via Sol-Gel Coating," *Advanced Materials Research*, vol. 667, pp. 128–134, Mar. 2013, doi: 10.4028/www.scientific.net/amr.667.128.